Heavy Flavour Benchmarks of ILD

Abstract

An overview of the performance of the ILD detector in its version Large and Small as relevant for the IDR is given

Contents

1. Introduction

Description of relevance of heavy flavour finals states for detector benchmarking

- Stringent test of (secondary) vertexing
- Exploitation of particle ID

2. Methods and tools

We use the following methods

- 'Core tools'
  - Jet algorithms at various steps of the analysis
  - Isolated Lepton Finding in case of $ee \to tt$ semi-leptonic
- Using TPC dE/dx to identify Kaons issue of the B-Meson decays (Processors????)
- Tools specific/developed for the study
  - Analysis of tracks associated to the secondary vertex (LCFIPlus v.xxxx and navigations through reconstructd particle list using LCRelations)
    - Purpose: Identify and add tracks that have not been associated in Standard Reco (VertexRecoveryProcessort)
- Quark charge measurement and corrections for miscalculations

- Probabilities on double charge measurements for $t\bar{t}$ and $b\bar{b}$ has been examined.
- Calculations scheme is shown below.

$$\left.\begin{aligned} N_{acc} &= Np^2 + Nq^2 \\ N_{rej} &= 2Npq \\ 1 &= p + q \end{aligned}\right\} \quad N_{corr} = N_{acc} \cdot \frac{p^2}{p^2 + q^2} \tag{1}$$

- where N is total number of events, N_{acc} and N_{rej} are number of events that were accepted and rejected, respectively. p and q values represents probabilities of events being accepted and rejected. Solving this equation will give us back both p and q, thus improving our results on A_{fb}.
- the correction has been applied to the $b\bar{b}$ studies while not in $t\bar{t}$. Selection scheme in $t\bar{t}$ is much more complicated than that for $b\bar{b}$ thus applying the correction will reduce the efficiency with little effect.
- Plots. $t\bar{t}$: Figure. 7, $b\bar{b}$: Figure. 7.

$e^-_L e^+_R \to b\bar{b}$ at 500 GeV

	IDR-L			IDR-S		
	Signal	$B_{b\bar{b}}/S$	$B_{rad.Z}/S$	Signal	$B_{b\bar{b}}/S$	$B_{rad.Z}/S$
Full sample	100.0%	1800.5%	359.1%	100.0%	1800.6%	359.0%
$b_{tag}(jet_1) > 0.9$ and $b_{tag}(jet_2) > 0.2$	70.2%	2.3%	147.7%	69.9%	2.3%	149.0%
$m_{jet_1+jet_2} > 200GeV$	68.2%	1.4%	6.7%	67.8%	1.2%	6.7%
$E_{photon} < 100GeV$	64.8%	1.3%	1.7%	64.3%	1.2%	1.6%

Table 1: Selection efficiency and B/S rejection for some bkg sources

2.1. Monte Carlo samples and Event processing

- specify samples that are used for the analysis
- Give list of processors that have been used, official reconstruction and private processors (Maybe summarised in a table). Document where to find them. Remark: this is maybe double work since on may give the processors already above.

3. Efficiencies and Control plots

- Common
  - it might be good to produce a plot of the b-momentum in the lab frame to point out the differences between the two final states.
  - Plots before and after vertex recovery (at least initially b and t analysis, large detector is enough unless striking difference).
  - Increase of purity by vtx recovery (b and t analysis, large detector is enough unless striking difference).
  - Detector acceptance (here maybe large and small) Slide 11 by Adrian
  - dE/dx including 'Jenny's' Plot, it's maybe sufficient to use the plots produced by Adrian.
- Information specific to tt-analysis
  - Energy and polar angle spectrum of selected isolated lepton
  - Table with selection efficiencies
  - For the record we may add the observation by Amjad on the b/c tagging.
  - Purity measurements for double charge selection + efficiencies of different methods.
- Information specific to bb analysis
  - Table with selection efficiencies
  - Is there anything specific to the bb analysis given that bb is a subsystem of tt?

3.1. Limits of $ee \to bb$ at 500 GeV

- Here I wanted to point out why the bb at 500 GeV is more involved than at 250 GeV but given the results shown today by Adrian this is maybe less of an issue.

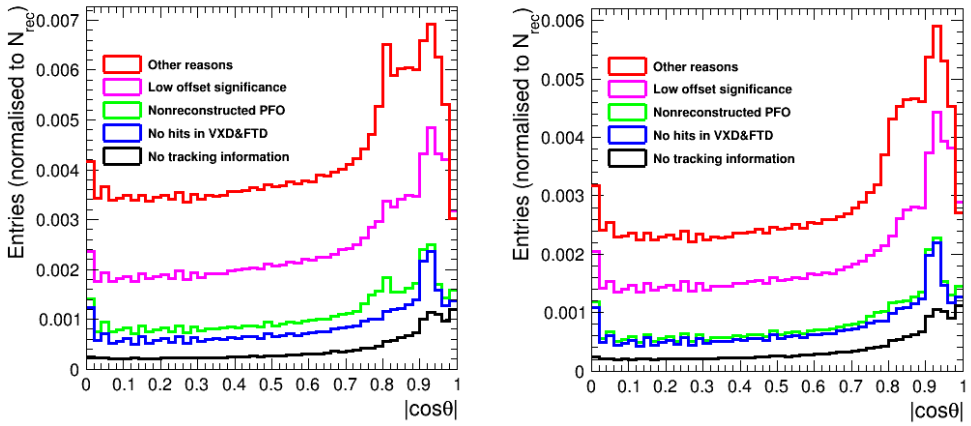

(a) Left, lost tracks in reconstructed vertexes before recovery. Right, lost tracks in reconstructed vertexes after recovery.

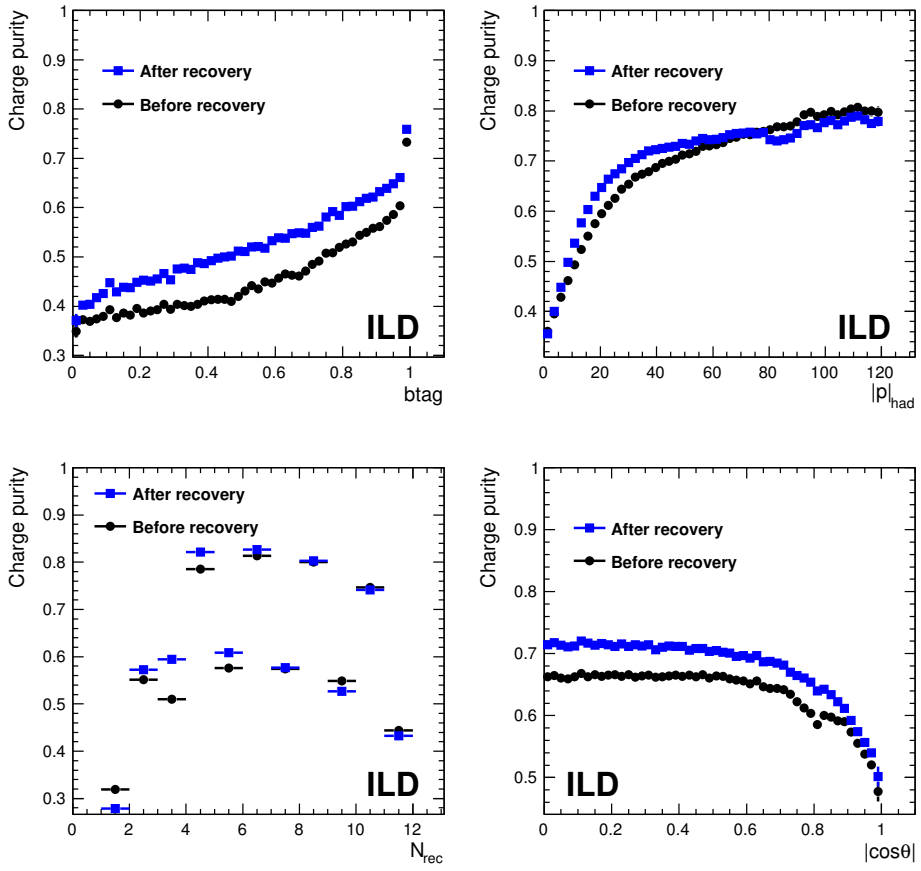

(b) Lower plot, B-quark charge purity in single jets as a function of different kinematic variables, after and before recovery.

Figure 1: $t\bar{t}$.

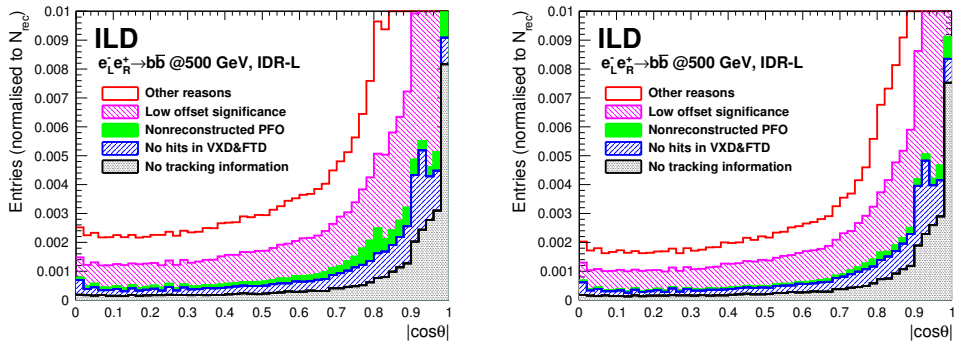

(a) Left, lost tracks in reconstructed vertexes before recovery. Right, lost tracks in reconstructed vertexes after recovery.

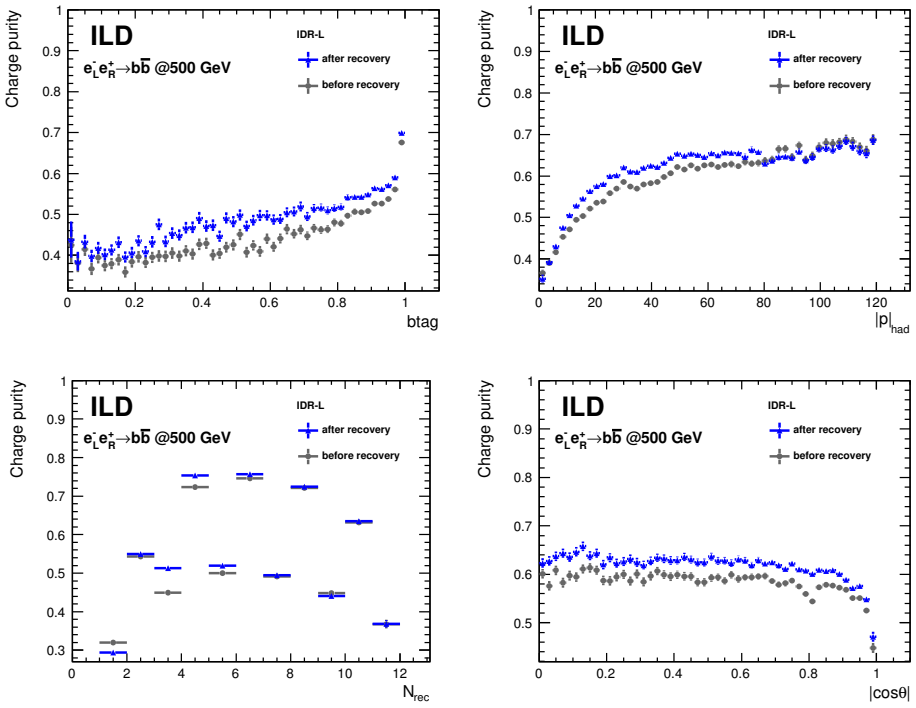

(b) Lower plot, B-quark charge purity in single jets as a function of different kinematic variables, after and before recovery.

Figure 2: $b\bar{b}$.

4. Results

- Polar angle spectrum $ee \to bb$ (Large and small)
- $ee \to tt$ including underlying b polar angle spectrum (Large and small)

5. Summary

The process $ee \to tt$ has been successfully ported from the 'DBD world' to the 'IDR World'. No major differences between short and large detectors.

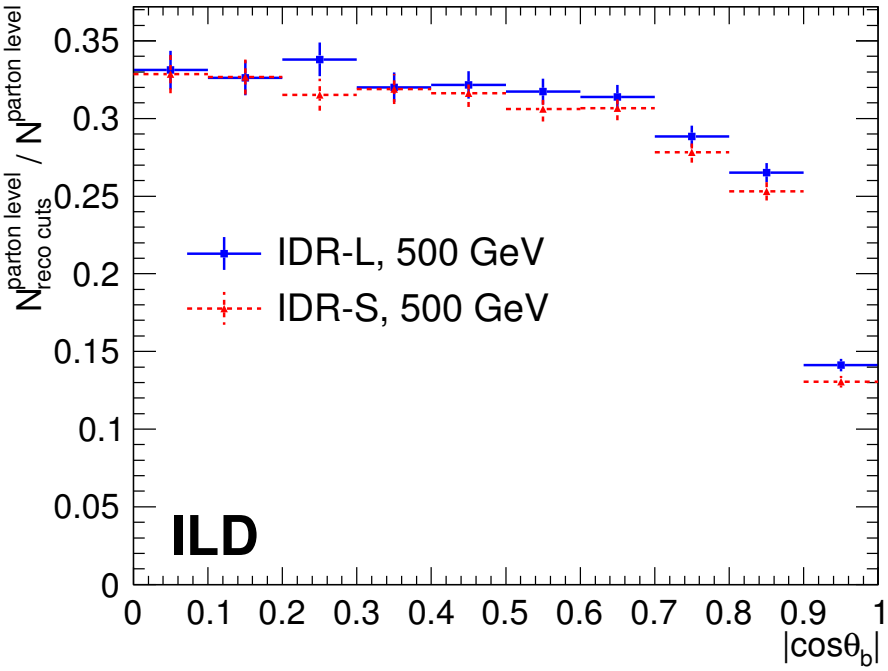

Figure 3: Detector acceptance distribution for b-tagged jets.

FURTHER SUGGESTIONS ARE WELCOME.

Acknowledgements

by the P2IO LabEx in the framework 'Investissements d'Avenir' managed by the French National Research Agency (ANR) under Grant Agreements ANR-10-LABX-0038 and ANR-11-IDEX-0003-01; by the 'Quarks and Leptons' Programme of CNRS/IN2P3 France; by the 'Prestige/MSCA Programme;

References

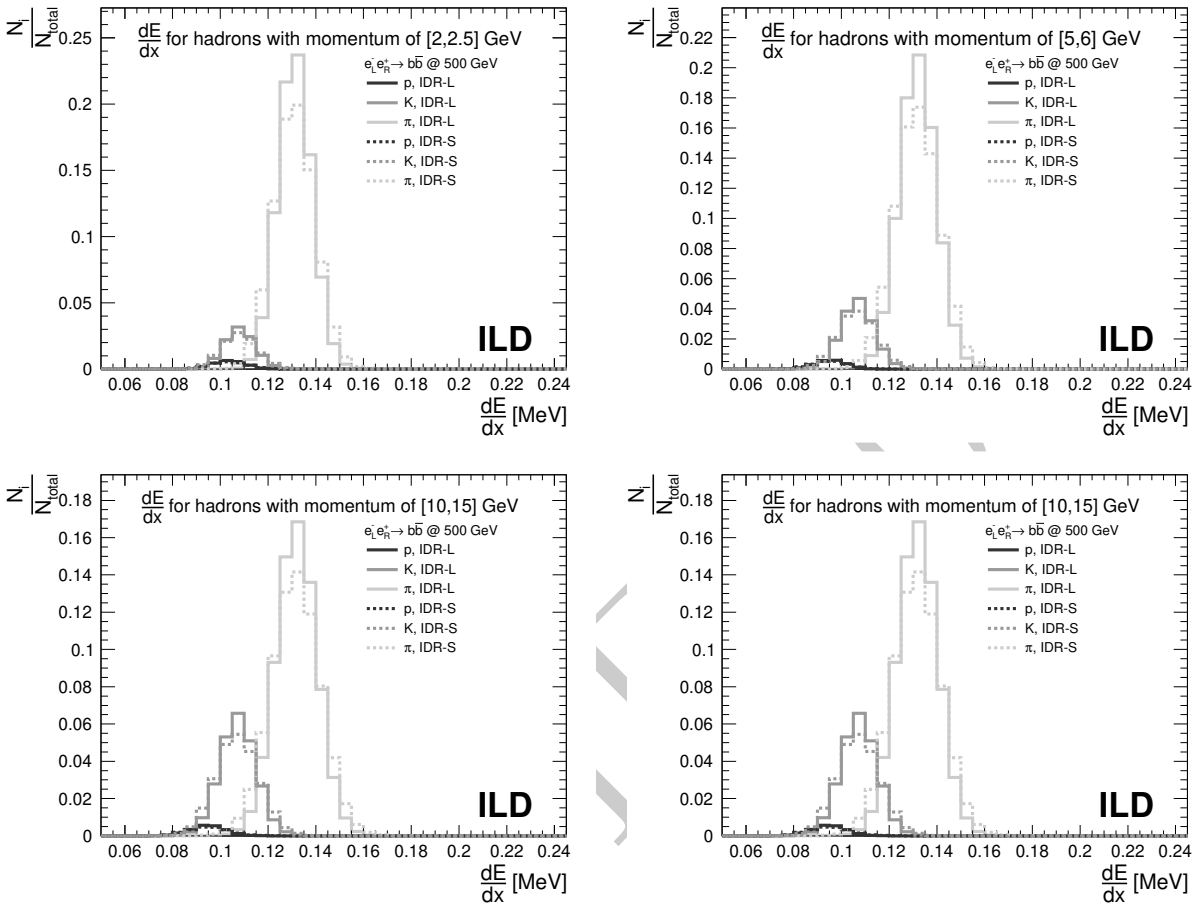

Figure 4: Projection of dE/dx for several momentum ranges. Comparison of hadron separation performance by different detector models in bbbar final states.

$e_L^- e_R^+ \to b\bar{b}$ at 500 GeV

	IDR-L	IDR-S
Vtx+Vtx	12.9%	12.8%
K+K	4.4%	4.0%
Vtx+K (diff. jets)	3.9%	3.7%
Vtx+K (same jet)	7.7%	7.4%

Table 2: Final selection efficiency, after double jet-charge measurement

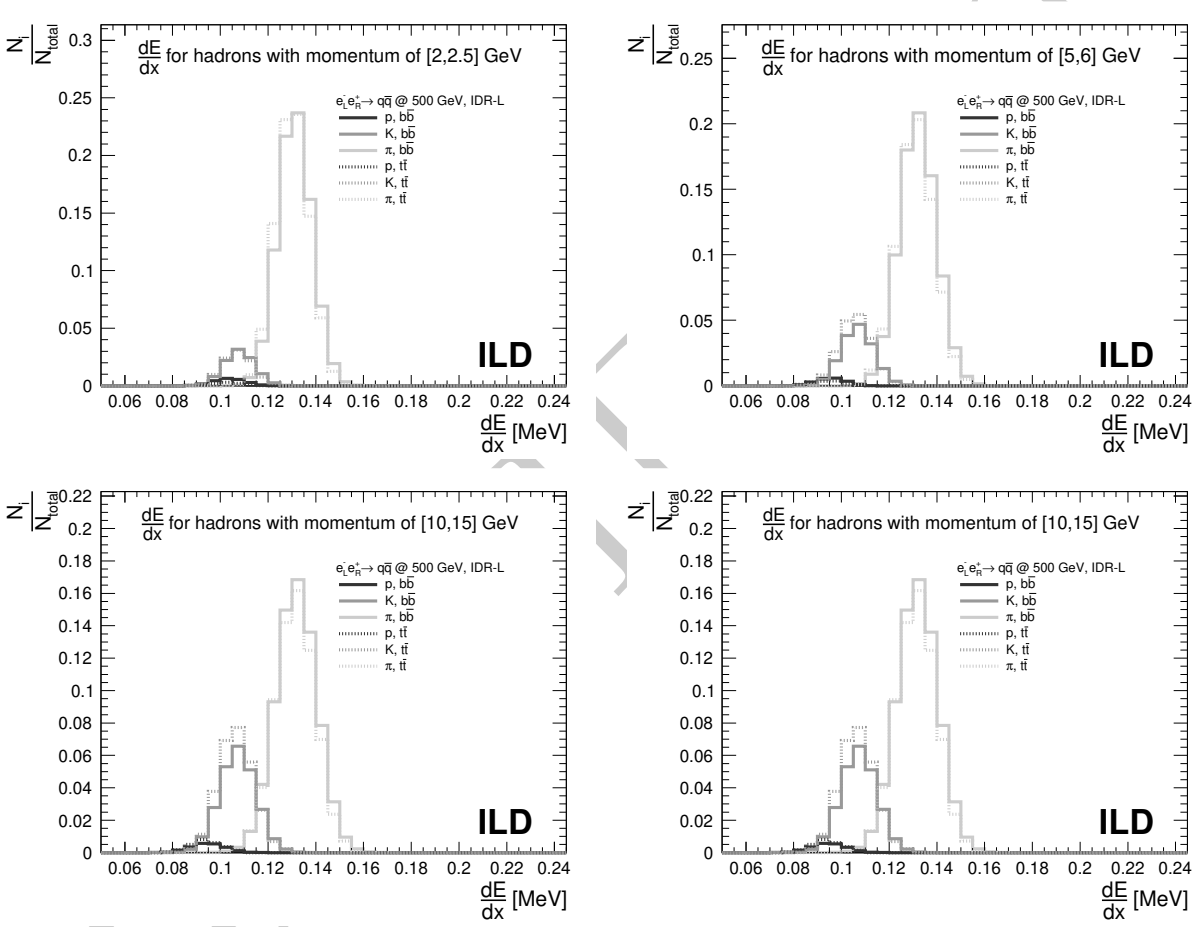

Figure 5: Projection of dE/dx for several momentum ranges. Comparison of hadron separation performance by the large model for different topologies.

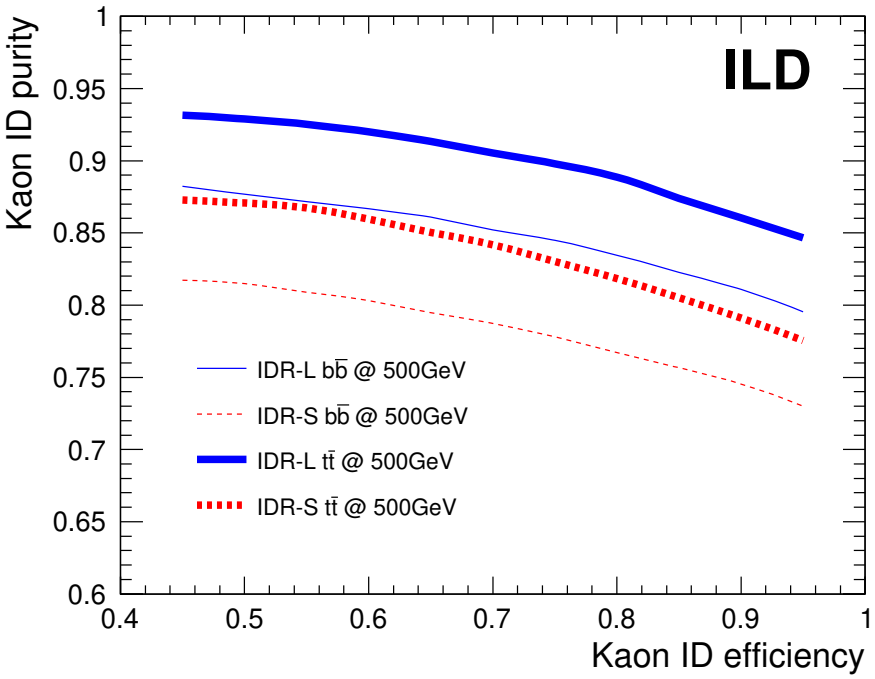

Figure 6

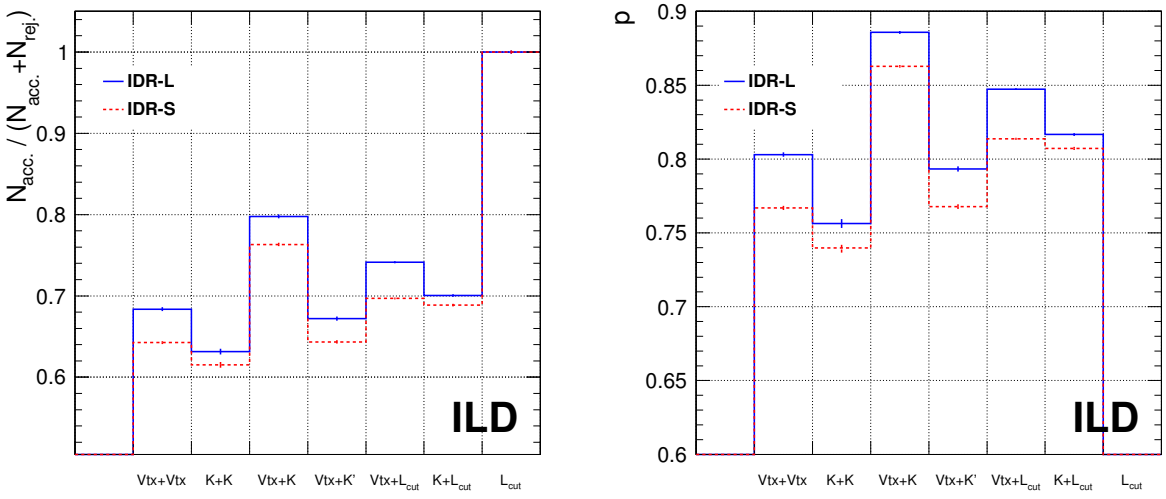

Figure 7: Calculated probability plots for $t\bar{t}$ events. Left plot shows the result of $N_{acc.}/(N_{acc.} + N_{rej.})$ and right plot shows the p values with different charge configurations.

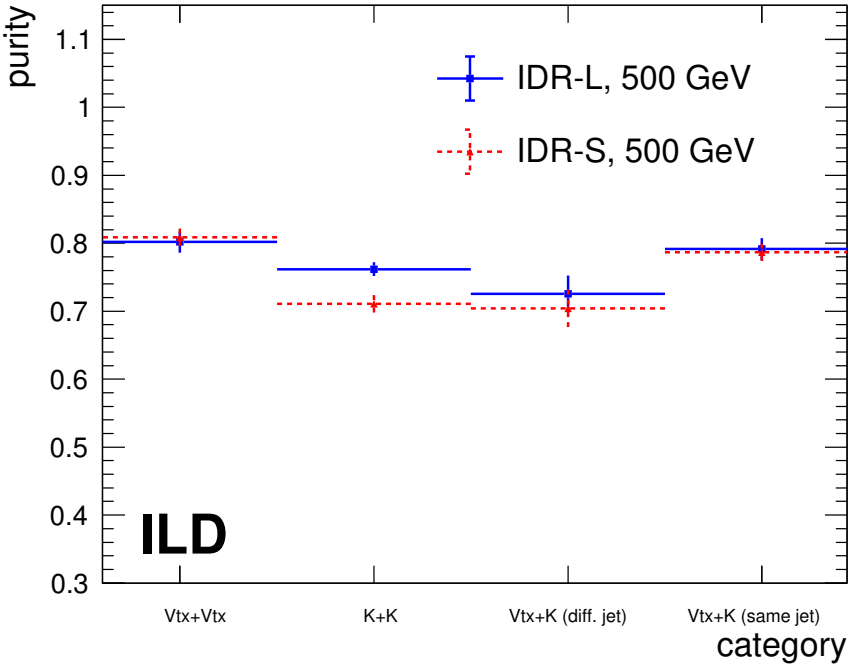

Figure 8: Purity of the different methods

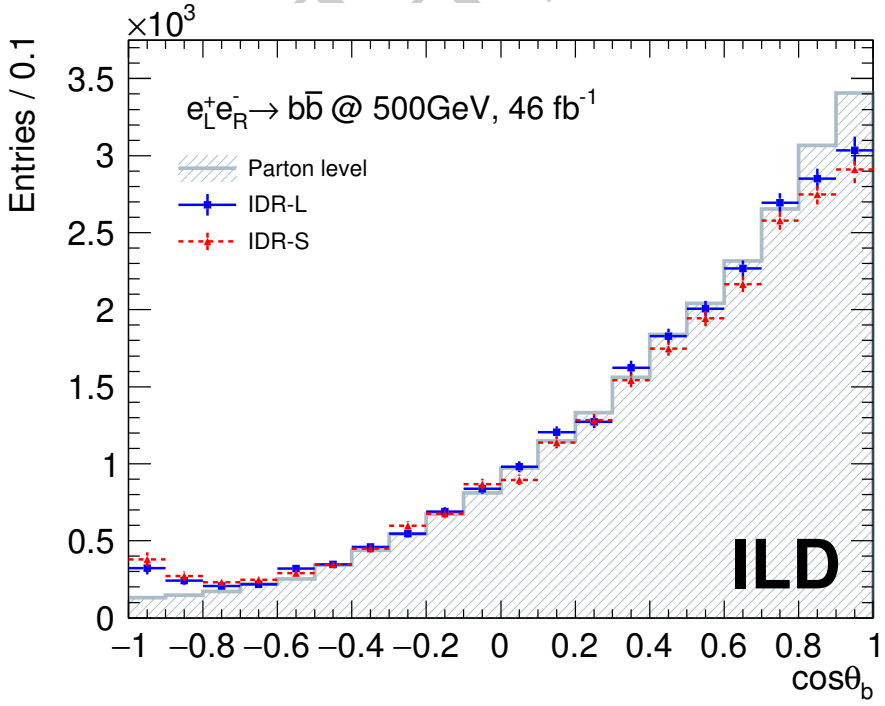

Figure 9

Analysis of $e^+e^- \to t\bar{t}$

- Settings
  - ILCSoft v02-00-02
  - Used yyxylv and yyxyev events (eliminated isolated tau)
  - Polarization of eLpR is used.
- Polar angle distribution of $t\bar{t}$
  - Full statistic polar angle
  - Polar angle distribution of $t\bar{t}$ of the generated and reconstructed data. Red dotted line shows the fitted result of the reconstructed events.
  - $t\bar{t}$ polar angle for large (l5) and small (s5) models. (Figure. 10)

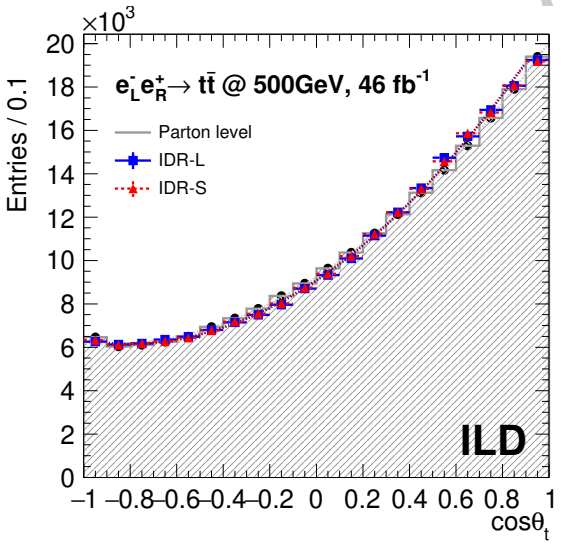

Figure 10: Polar angle distribution for top quark. Distributions for IDR-S is normalized to the one for IDR-L so that both histograms will be on the same level.

  - Final efficiencies

Afb gen	0.328288	N: 1351248
Afb reco	0.338966	N: 210334
Final efficiency	31.1318%	

Table 3: l5 final efficiency and A_{fb}

Afb gen	0.328233	N: 1418738
Afb reco	0.338662	N: 219177
Final efficiency	30.8975%	

Table 4: s5 final efficiency and A_{fb}

  - No significant differences were confirmed between s5 and l5 samples. For the $t\bar{t}$ studies, we see that the polar angle distribution is consistent with the Parton level result. At the edges of the polar angles, we do not see inefficiencies due to the detector geometry. Inefficiencies of at the edges of the detectors originates from inability to reconstruct b jets going to the forward region. For the top pair reconstruction, we can also rely on W informations thus not losing much efficiencies at the edges.

- Polar angle distribution of $b\bar{b}$
  - Full statistic polar angle
  - We could put each figures side by side for comparison. For example, we can put $t\bar{t}$ and $b\bar{b}$ plots side by side with same detector model.
  - $b\bar{b}$ polar angle for large (l5) and small (s5) models (Figure. 11)

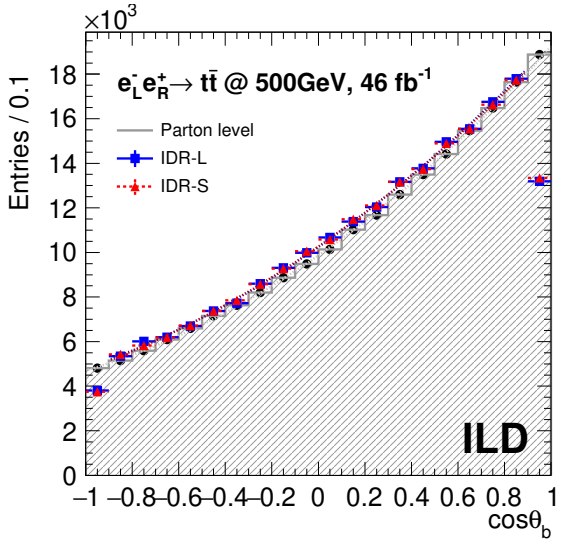

Figure 11: Hadronic polar angle distribution. Distributions for IDR-S is normalized to the one for IDR-L so that both histograms will be on the same level.

- Others

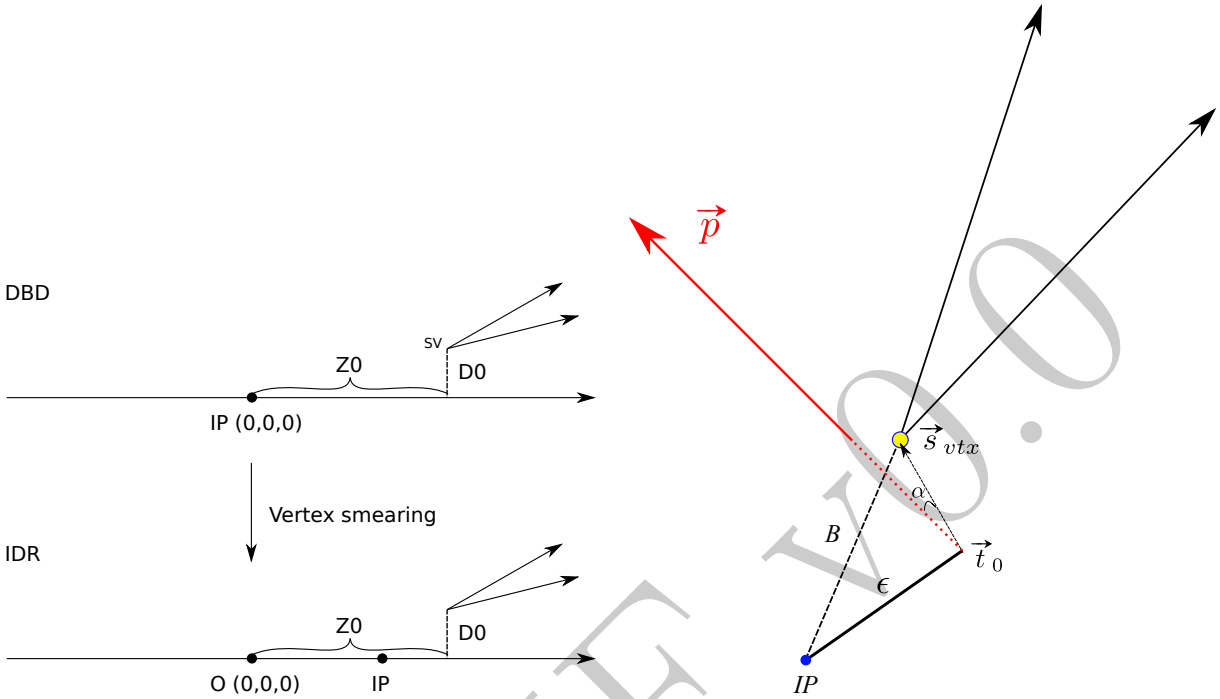

Figure 12: Left is